Chapter 10

Diameter Measurement of Spherical Objects

10.1 Introduction

10.1.1 Context: grinding field and robotics

The particular problem addressed here is the noncontact diameter measurement of spherical objects. An application can be found in the grinding field, where balls are used for crushing materials. Our method could be used in this case to control their worn state.

Ambulatory inspection, namely in a robotic environment, is another field of application, which requires the availability of a whole set of new sensors able to detect and characterize the shape of diverse mechanical pieces. Sorting spherical pieces of different diameters or nuclear decommissioning (where vessels topped by semispherical caps are often encountered) are here of concern.

Another interest of this study is that, as far as we know, it gives for the first time a solution for the in-situ noncontact measurement of spherical objects.

This chapter is a direct extension of Chapter 9. The purpose of this new application is to verify that the "three-tangent method" developed in the case of cylinders remains pertinent in this new context of spherical objects, and more particularly that it is at least as efficient as the classical gradient descent method, proposed in alternative.

We present the developments, results and conclusions of this study, for which the objective is to achieve a maximum relative error on the diameter of 1%, for diameters ranging from 10 to 50 cm. These figures have been chosen because, to our opinion, they would meet the industry's requirements in the two fields of application mentioned hereabove. The distance range is fixed to 0.5–2 m.

10.1.2 Organization

This chapter is organized in an intuitive way. At first, the instrument is presented in Section 10.2.

After a short description of the image processing algorithm (Section 10.3), we present the extension of the "three-tangent method" used for the determination of the radius of the sphere (Section 10.4).

The next section details an alternative method, based on gradient descent, implemented to verify the performance of the "three-tangent method" (Section 10.5).

In Section 10.6, we make some comment on the error that one can expect on the radius, using the accuracy analysis of Chapters 7 7 and 9.

The three last sections present the experimental results we obtained on a pre-prototype setup (Section 10.7), explain what would have occurred if our theoretical models were not so refined (Section 10.8), and give some conclusions (Section 10.9).

Note that the present chapter groups and develops one paper previously published [49] and an other accepted for publication [50]. They were both inspired by [51].

10.2 Description of the Instrument

The instrument used is sensibly the same as that described in Section 9.7.

Let the target under test have an arbitrary position with regard to the (x, y) plane of a monochrome CCD camera observing the scene (Fig. 10.1). Systems of reference (x, y, and z) and (x_{pix}, y_{pix}) are as defined in Chapter 2. For convenience, the camera plane will often be represented as horizontal, but of course is it not mandatory.

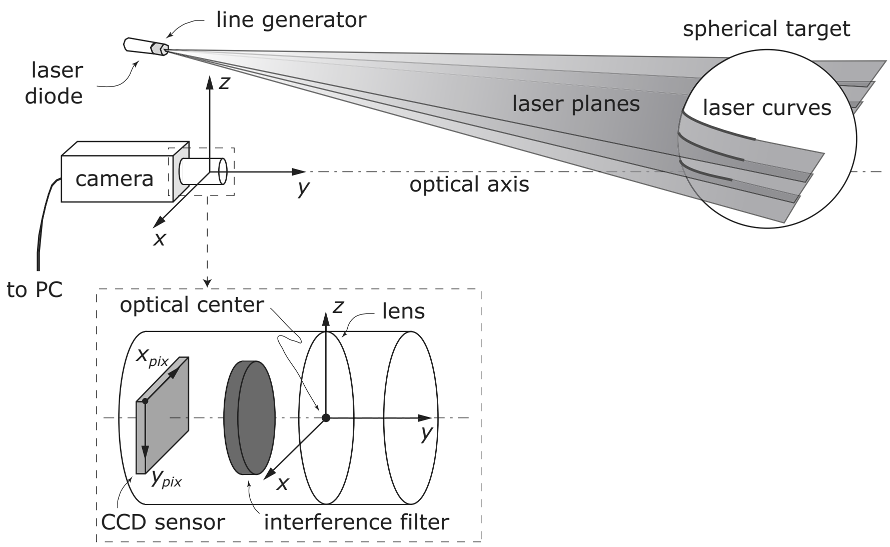

Fig. 10.1. Configuration of the device. 3-D view.

The object, supposed perfectly spherical, is illuminated by multiple laser planes slightly tilted in the y direction on the camera plane, creating curved lines on the target. We will prove that two laser planes are a minimum and that the higher the amount of planes, the better the accuracy but also the computing complexity. A number of three planes seems to be a good compromise.

The surface of the target is supposed at least partially diffusing, so that in any case, the camera receives a part of each plane luminance. As in Section

9.2, we suppose that the portion of the sphere illuminated by each laser plane is at least equal to that seen by the camera.

A narrow-band interference filter described in Chapter 4, centered on the wavelength of the laser diode, is placed between the CCD sensor of the camera and its objective, in order to increase the contrast between the curve to be extracted and the rest of the scene.

Our instrument is defined by twelve parameters: seven for the camera (see Chapter 2) and—in principle—three for each laser plane i. We nevertheless suppose that angles ϵ_i are identical for the three laser planes (which is appropriate seen the high quality of the laser optics; we note it ϵ). This explains why the instrument has twelve parameters and not fourteen (see Fig. 3.6, where only one laser plane is represented, and Section 3.5). Distances e_i are intentionally limited to about 10 cm to maintain the compactness and the ambulatory nature of our instrument. Tilt angles δ_i and the zoom factor of the camera (adjusted mainly by changing the focal length) are chosen so that the instrument covers the distance and angle ranges for the concerned application (i.e. the laser lines must stay in the field of view of the camera in any case).

The two distinct procedures described in Chapter 6 are used to calibrate the instrument, the laser plane calibration being performed on known spherical objects (even though mentioned here, the latter can obviously not be performed until the radius calculation method has been chosen; see Sections 10.4–10.5).

10.3 Image Processing

An image processing algorithm extracts the laser curves intersected by the sphere by isolating them from the rest of the scene. The interference filter carries out a substantial part of the task, but some additional treatments on the image are still needed to eliminate the noise surrounding the curve.

These are (see Chapter 5 for a description of each item):

- subtraction of two pictures sequentially taken (one with the laser diode on, the other with the diode off);
- thresholding;
- segmentation;
- laser curve selection;
- column-by-column subpixel location of the curves;
- correction of the distortion.

The output of this algorithm consists of three lists containing the coordinates in the ICS of all the pixels belonging to each laser curve.

10.4 Radius Calculation #1: the "Three Tangent Method"

As shown in Chapter 3, a one-to-one correspondence exists between the ICS coordinates of any pixel of the laser curves and the WCS coordinates of the corresponding point in the scene.

We can thus assess that the coordinates of every point of the laser curves are known in the WCS by (3.7).

In Chapter 9, the radius calculation of a cylinder was performed by mean of what we called the "three-tangent method," based on the property that a circle is entirely defined by three of its tangents. We showed that this method is the most robust one for cylindrical objects, taking into account the laser lines' particular characteristics (see Section 9.5).

In the case of a sphere, three portions of nonparallel circles are generated by the intersection of the laser planes with the object. Their radii generally have nonequal values (excepted in some rare—but not problematic—cases where two radii are equal). Note that from now on, for sake of easiness, we will speak of circles instead of circular portions, the first being the closed form of the latter.

Since the geometry of these laser curves is similar to that observed in the case of the cylinder, one is inclined to assume that the "three-tangent method" keeps its pertinence for accurately determining the radii of these circles and consequently the radius of the sphere. This is what we will prove.

Let us define the new orthogonal coordinate systems (x_i, y_i, and z_i) aligned with each laser plane, with axes x_i and y_i belonging to the concerned plane. They are obtained by translating the original system of distance e_i along z-axis and then double-rotating it around x (by angle δ_i) and the new y (by angle ϵ) axes. The relations expressing these new systems in function of the original one are:

$$\left\{\begin{array}{l} x_i = x\cos\epsilon - y\sin\delta_i\sin\epsilon + (e_i - z)\cos\delta_i\sin\epsilon \\ y_i = y\cos\delta_i + (e_i - z)\sin\delta_i \\ z_i = x\sin\epsilon + y\sin\delta_i\cos\epsilon + (z - e_i)\cos\delta_i\cos\epsilon \end{array}\right. \tag{10.1}$$

Each circle i generated by laser plane i is in the (x_i, y_i) plane of the coordinate system attached to the corresponding laser plane (see Fig. 10.2), and is completely defined by the three tangents $O_iP_{2',i}$ and $O_iP_{3',i}$ issued from the origin O_i and $P_{2',i}P_{3',i}$ aligned with x_i. To find its radius, as detailed in Section 9.4, we only need the y_i coordinate $Y_{1,i}$ of point $P_{1,i}$ and the x_i coordinates $X_{2',i}$ and $X_{3',i}$ of points $P_{2',i}$ and $P_{3',i}$. These can easily be found from the image plane using (3.7) and (10.1). Radius R_i is then [cf. (9.4)]:

$$R_i = \frac{Y_{1,i}\left(X_{3',i} - X_{2',i}\right)}{\sqrt{X_{2',i}^2 + Y_{1,i}^2} + \sqrt{X_{3',i}^2 + Y_{1,i}^2} - \left(X_{3',i} - X_{2',i}\right)} \tag{10.2}$$

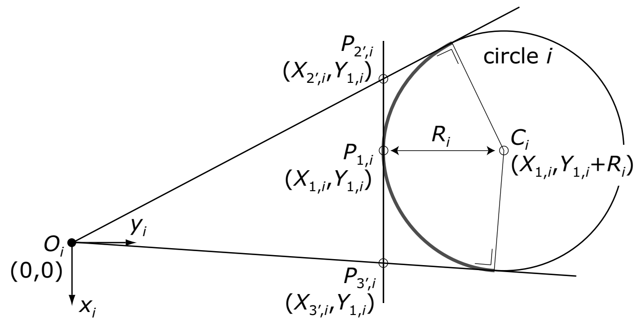

Fig. 10.2. "Three-tangent method." View in the $(x_i,\, y_i)$ plane.

Let us now consider the couple of laser planes 1–2. On Fig. 10.3 representing the geometry in the (y_2, z_2) plane of the two circles that they are generating on the sphere, we can see that:

$$\begin{aligned} R^2 = R_1^2 + r_1^2 &= R_2^2 + r_2^2 \\ D_{12} = r_1 \cos\delta_{12} &+ r_2 - R_1 \sin\delta_{12} \end{aligned} \tag{10.3}$$

where R is the searched radius of the sphere, $\delta_{12} = \delta_2 - \delta_1$ and D_{12} is the z_2 coordinate of $P_{1,1}$. Its expression is [see (3.7) and (10.1)]:

$$D_{12} = X_{1,1} \sin\epsilon + Y_{1,1} \sin\delta_2 \cos\epsilon + (Z_{1,1} - e_2) \cos\delta_2 \cos\epsilon \tag{10.4}$$

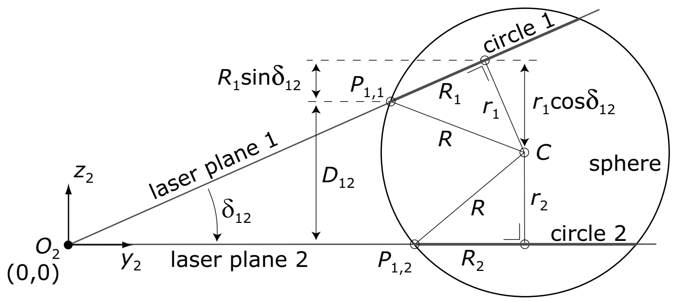

Fig. 10.3. Geometry of the two circles 1–2 and the sphere. Cut in the $(y_2,\, z_2)$ plane.

Remark that D_{12} is the only additional quantity to be measured in comparison with the original "three-tangent method." Nevertheless observing (3.7) and (10.4) we see that no other pixel coordinates need to be known. We thus do not expect supplementary uncertainties in the final result than in the original method.

Relations (10.3), taking (10.2) into account, form a system of three equations of unknowns R, r_1 and r_2, the solution of which finally leads to the searched quantity R (positive root of a second degree equation). One finds:

$$r_1 = \frac{\sqrt{R_2^2 \sin^2 \delta_{12} + 2D_{12}R_1 \sin \delta_{12} + D_{12}^2} - R_1 \cot \delta_{12} - D_{12}}{\sin^2 \delta_{12}} \tag{10.5}$$

and thus the radius R of the sphere is:

$$R = \sqrt{R_1^2 + r_1^2} \tag{10.6}$$

Even if two laser planes are thus theoretically sufficient to determine the sphere radius R, two more expressions of R similar to (10.5) and (10.6) can be found by considering the two other couples of laser planes (1–3 and 2–3), permitting us to enhance the accuracy on R by taking the average value.

10.5 Radius Calculation #2: the Gradient Descent Method

In order to evaluate the efficacy of the “three-tangent method,” we compare it to a second technique, based on the gradient descent method (see also [52]). It is also used for the laser plane calibration of the instruments presented in this work, and is detailed in Section 6.3.2.

The three laser curves are providing us—using (3.7)—with a large collection of N points P_j theoretically belonging to the sphere, and satisfying the equations in the WCS ($j = 1 \ldots N$):

$$(X_j - X_C)^2 + (Y_j - Y_C)^2 + (Z_j - Z_C)^2 - R^2 = \Delta_j \tag{10.7}$$

where X_C, Y_C and Z_C are the coordinates of the sphere center C; X_j, Y_j and Z_j are the coordinates of P_j; Δ_j is an indication of the gap between P_j and the sphere surface, coming e.g. from quantization or measurement errors.

If we considering both the center coordinates and the radius as the parameters to optimize, gradient descent method will lead to an estimate of these such that the mean error Δ_j in the N equations (10.7) is minimized.

As specified in Section 6.3.2, the method requires an initial estimation of the parameters. We use:

$$\begin{array}{rcl} X_{C,0} & = & X_{j,\mathrm{mean}} \\ Y_{C,0} & = & \max Y_j \\ Z_{C,0} & = & Z_{j,\mathrm{mean}} \\ R_0 & = & \max Y_j - \min Y_j \end{array} \tag{10.8}$$

Note on the choice of the method

Gradient descent is an iterative technique, with all the drawbacks implied by this type of method (unknown, sometimes longer computation times, need of an initial estimation, convergence conditions...).

Since—as suggested by (10.7)—the partial derivatives of Δ_j in relation to the parameter vector are linear, one could avoid the aforementioned drawbacks by opting for an analytical method, like the pseudo-inverse one [29].

Nevertheless such a technique would require the inversion of large matrices, which is very difficult to implement in C++, the computer language we use. Moreover it would eventually produce the same results as the gradient descent method.

It is thus not developed here.

Note on the calibration of the instrument

As said above, the camera and laser plane parameters are determined through two distinct calibration procedures.

The first operation concerns the camera parameters and causes no particular trouble. The second one though, concerning the laser plane parameters, requires some precautions.

In this particular application, it is done on two known spherical objects, at various distances, and it also relies on the gradient descent method, where the criterion to minimize is the mean relative error ρ_R on the radius. The parameter vector to optimize is $U_l = (e_1, e_2, e_3, \delta_1, \delta_2, \delta_3, \epsilon)$.

Since our second radius calculation method uses the same optimization technique, some precautions are to be taken. Actually, two sets of parameters are to be optimized. Performing one global gradient descent on both sets would lead to parameters that are incoherent with regard to the real physical configuration of the instrument. We rather have to execute the two descents sequentially, switching back from one to the other a few times if necessary.

10.6 Expected Accuracy

Similarly to the previous chapter, an analytical study of the accuracy on the radius that one can expect would be very tedious. Unfortunately, contrarily to the cylinder application, there are no simplifications that could be introduced to make the developments easier.

We will therefore limit ourselves to give the same comment than in Section 9.11, regarding the passage from the particular case of a transversal, centered cylinder to the general situation of a randomly tilted object: as no additional quantities (compared to Chapter 9) are required to be measured on the image, we can expect a similar accuracy, i.e. about 1.2% at worst. This will actually be corroborated by our experiments in the next section.

10.7 Results

The same PC-connected pre-prototype than in Chapter 9 was used. See Section 9.12 for more details.

As a matter of example, Fig. 10.4 shows the photograph of a typical scene acquired by the camera. The sphere, consisting in a rubber basketball ball, is placed in a clear room, in front of a wall. The raw image, obtained before the processing, is on the left. The additional lines of lower luminance clearly visible on the sphere are due to a grating effect of the laser optics, generating superior diffraction orders. These lines, together with the segments out of the sphere, disappear after data processing (right image).

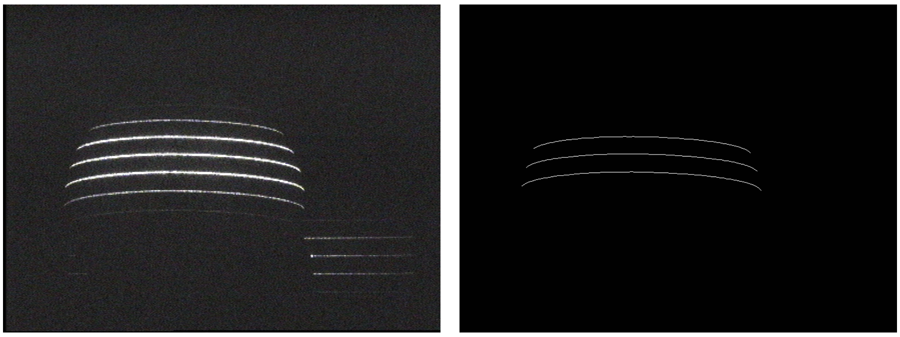

Fig. 10.4. Example of observed scene. The raw image is on the left, the same picture after image procession being on the right.

We made a measurement campaign of 70 experiments, in a clear room, on two spherical objects of different radii (6.5 and 13 cm) and at various aims and distances between the operator and the object (up to 2.5 m). The same flexible steel measuring tape than in Chapter 9 was used to determine these radii, with an estimated accuracy of 0.1 mm (see Section 9.12.1).

The results we obtained with the two radius calculation methods are presented on Fig. 10.5 showing histograms of the relative error ρ_R on the radius, TABLE 10.1 giving recapitulative figures (where the two first lines present the percentage of measurements for which $|\rho_R|$ is below 1 and 1.5% respectively; ρ denotes a relative error and σ a standard deviation), and Fig. 10.6 detailing the results of 19 measurements on the 6.5-cm-radius sphere. They are fully conclusive as the majority of the measurements presents a relative error ρ_R below 1%.

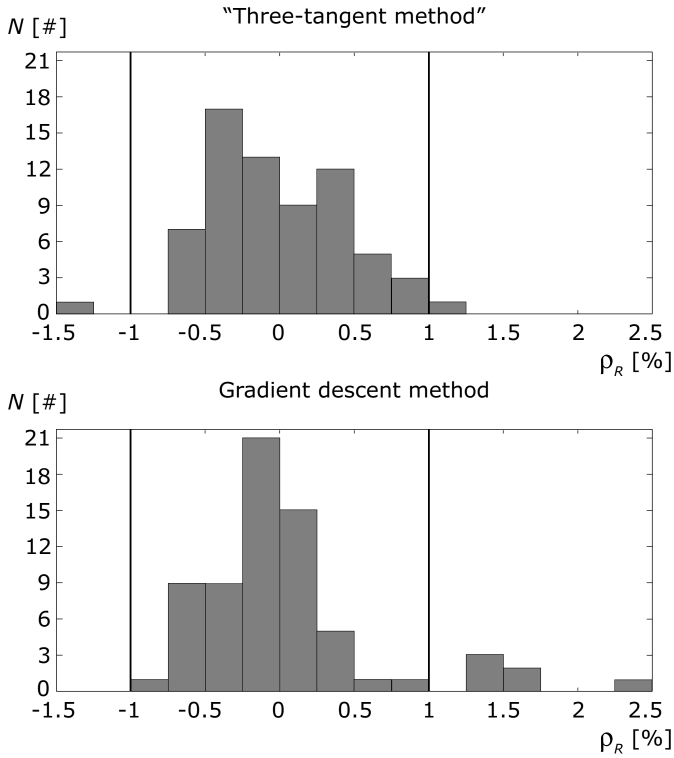

Fig. 10.5. Histograms of the relative error on the sphere radius.

Beside that, one sees that both methods are efficient, but that the "three-tangent method" shows the best results:

- A greater proportion of measurements have a relative error below 1% (97% against 91%);
- Its histogram is less spread and thus its standard deviation smaller (0.46% against 0.60%);
- It behaves better when the object is more distant. Fig. 10.6 clearly shows the limits of the gradient descent method when the distance rises. This is due to the fact that the laser curves in the image tend to become straight lines when the object goes further, because of a loss of resolution at large distance. This leads to a bad estimation of the P_j coordinates, which has a severe influence on the computed radius (it would be infinite for

Table 10.1. Recapitulative Figures for Both Methods

	"Three-tangent"	**Gradient descent**
$\lvert\rho_R\rvert$ <1%	97%	91%
$\lvert\rho_R\rvert$ <1.5%	100%	96%
$\rho_{R,\text{mean}}$	−0.01%	0.04%
σ_{ρ_R}	0.46%	0.60%

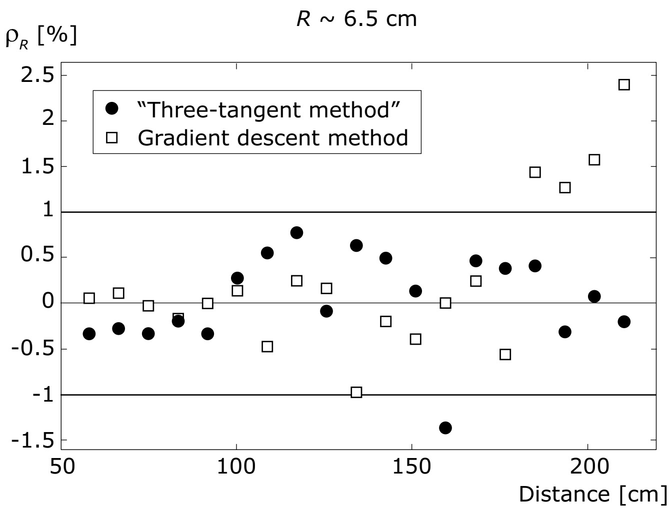

Fig. 10.6. Results of measurements taken on a spherical object at various distances.

strictly straight lines). The three-tangent method is not affected by this, as shown in Section 9.5, since it uses robust coordinates independent of the shape.

Its other advantages are its easiness of implementation, its shorter, known and constant calculation time and the fact that no initial estimation of the sphere geometry is needed[1].

10.8 Without a Refined Theory...

The similarities between the cylinder application of Chapter 9 and the present one allows us to make the same comments than in Section 9.13, regarding what would have happened if our theoretical models were not so complete. The only difference is that in this sphere application, no curve smoothing is required, since the objects were all *smooth* (at the scale of the camera field-of-view).

We can thus claim again that without such a complete theoretical basis, one would never have reached such good performances.

10.9 Conclusions

The feasibility of a new method for the diameter measurement of spherical objects was studied. The innovative character of our instrument is again to be found in the "three-tangent method" for the robust determination of the radius of a circle. We previously showed that it is the best computation method for the cylinder diameter determination and we extended it to the case of a sphere. As far as we know, it is the first time that a solution is brought for the in-situ noncontact diameter measurement of spherical objects.

Our results allow us to claim that a general accuracy of about 1% on the diameter of the measured objects is achieved for diameters ranging from 10 to 30 cm and for a distance—a priori not known—between the instrument and the spherical object going up to 2.5 m. This performance is in agreement with our objective, mentioned in Section 10.1.1, and is comparable to that of our method studied in Chapter 9, where the object was a cylinder. The extension of the "three-tangent method" has thus obviously succeeded.

It is foreseeable that a similar accuracy would be achieved for smaller spheres (e.g. of a few mm) at rated maximal distance (a few tens of cm) by equipping the camera with an appropriate lens, extending in such a way the method to the radius determination of balls for bearings (if we can suppose the ball surface at least partially diffusive).

---

[1] See the note on the choice of the "statistical" method in Section 10.5 to see how these drawbacks could be avoided

As shown in this chapter, our method reaches better performances than a systematic, statistical and heavy-to-manipulate technique like the gradient descent. It is a very important element in the portability context, together with the simplicity of our instrument and the low cost of its components, as mentioned in Section 9.14.